energies

MDPI

Article

Impact of Preparation Method and Y_2O_3 Content on the Properties of the YSZ Electrolyte

Michal Carda, Nela Adamová, Daniel Budáč, Veronika Rečková, Martin Paidar * and Karel Bouzek

Department of Inorganic Technology, Faculty of Chemical Technology, University of Chemistry and Technology, Prague, Technická 5, Prague 6—Dejvice, 166 28 Prague, Czech Republic; cardam@vscht.cz (M.C.); adamovae@vscht.cz (N.A.); budacd@vscht.cz (D.B.); reckovav@vscht.cz (V.R.); bouzekk@vscht.cz (K.B.)
* Correspondence: paidarm@vscht.cz; Tel.: +420-220-443-802

Abstract: This study is an effort to cover and interconnect multiple aspects of the fabrication of the yttria-stabilized zirconia (YSZ) from powder preparation to a solid electrolyte suitable for utilization in solid oxide cells. Thus, a series of YSZ electrolytes was prepared, differing in the content of the Y_2O_3 dopant and in the method of preparation. Combustion synthesis along with the thermal decomposition of precursors was used for YSZ powder synthesis with a dopant content of 8 to 18 mol.%. Post-synthesis treatment of the powder was necessary for achieving satisfactory quality of the subsequent sintering step. The morphology analyses of the YSZ powders and sintered electrolytes produced proved that small particles with a uniform size distribution are essential for obtaining a dense electrolyte. Furthermore, the conductivity of YSZ electrolytes with different Y_2O_3 contents was examined in the temperature range of 400 to 800 °C. The lowest conductivity was found for the sample with the highest Y_2O_3 content. The obtained results enable the preparation methods, YSZ powder morphology, and composition to be connected to the mechanical and electrochemical properties of the YSZ electrolyte. Thus, this study links every step of YSZ electrolyte fabrication, which has not been sufficiently clearly described until now.

Keywords: solid oxide cells; yttria-stabilized zirconia; YSZ; powder synthesis; dopant content; shape molding; conductivity

Citation: Carda, M.; Adamová, N.; Budáč, D.; Rečková, V.; Paidar, M.; Bouzek, K. Impact of Preparation Method and Y_2O_3 Content on the Properties of the YSZ Electrolyte. *Energies* **2022**, *15*, 2565. https://doi.org/10.3390/en15072565

Academic Editors: Stephen McPhail and Vladislav A. Sadykov

Received: 9 February 2022
Accepted: 29 March 2022
Published: 1 April 2022

1. Introduction

Solid oxide cells (SOCs) have been the subject of intensive research in recent decades, as a promising technology for sustainable energy conversion. This technology has a crucial role in the hydrogen economy concept, which is a set of technologies allowing the highly efficient utilization of renewable energy sources characterized by the intermittent production of green energy. The main benefit of SOCs originates from the high operating temperature (400–800 °C), which ensures rapid electrode reaction kinetics, the operational reversibility of the system, and efficient utilization of the heat produced. Moreover, the efficient utilization of complex reactions, such as CO_2 and steam co-electrolysis under syngas formation, is also feasible, in contrast to similar technologies. At the same time, because of the high operating temperature, the utilization of platinum group metals can be avoided. However, high temperatures also pose a significant challenge for the selection of suitable materials, which must be chemically and thermally stable and, above all, thermomechanically compatible with each other.

Components of the membrane–electrode assembly (MEA) of SOCs are prevalently based on various oxides [1–7]. A single MEA comprises a single electrolyte and two electrodes located on its sides, with the possibility of additional interlayers to prevent undesired interactions of the individual components. In the case of an electrolyte-supported cell, the electrolyte represents the thickest component, and is therefore directly responsible for the decisive part of cell ohmic losses. Therefore, a material with high ionic conductivity is

needed to reduce this particular process efficiency loss. Despite the rapid development of new materials, yttria-stabilized zirconia (ZrO_2—Y_2O_3; YSZ) is still among the most important materials for high-temperature solid ion-conducting electrolytes [8–10]. YSZ electrolytes represent an inexpensive, nonporous, gas-tight and stable material, characterized by very good ion conductivity [11]. For applications in SOCs, its thermomechanical compatibility with the majority of electrode materials is also important [12–14]. The ionic conductivity of YSZ is based on the motion of oxygen vacancies through its crystalline structure. These vacancies originate from a partial substitution of quadrivalent Zr^{4+} ions in the cubic ZrO_2 lattice by the trivalent Y^{3+}. The amount of Y_2O_3 dopant directly determines the ionic conductivity and stability of YSZ [15–19]. The very low content of Y_2O_3 leads to high mechanical stability of the resulting materials, at the cost of its reduced ionic conductivity. On the other hand, an overly high dopant concentration also results in reduced ionic conductivity of the electrolyte. This is caused by the increased affinity of the oxygen vacancies and dopant cations, resulting in defects with low mobility [20]. Additionally, it causes limited thermal stability of the resulting YSZ. The optimal amount of dopant in YSZ is in the range of 8–10 mol.%, which exhibits high ionic conductivity and satisfactory stability [15,20]. Due to the wide range of YSZ applications, ranging from SOCs and oxygen sensors to technical ceramics, YSZ powders are commercially available, albeit limited only to the most commonly required concentrations of Y_2O_3 (i.e., 3 and 8 mol.% of Y_2O_3) [11]. This could be very limiting, because the development of SOCs often demands specially tailored YSZ with particular properties.

Therefore, YSZ electrolytes with a desired Y_2O_3 content different from those available commercially have to be prepared in-house. In the past, numerous authors have published articles regarding YSZ powder or electrolyte fabrication. However, they generally share a common flaw, because they focused their attention only on a particular step in the fabrication process. These published works could be sorted to powder [21–24] or electrolyte fabrication [25–28], and the characterization of YSZ with various dopant contents [15,16,29–31]. The entire process and significance of its individual steps with respect to the resulting materials has, however, not yet been described. This is an important aspect for obtaining reproducible and directly comparable results reached by the individual authors. The present study aims to address this major shortcoming by featuring the whole fabrication process and cell examination. Individual steps of the YSZ electrolyte fabrication are identified and described, together with their impact on the properties of the resulting YSZ electrolyte. Neglecting particular material properties or process conditions could lead to decreased cell performance, mechanical stability issues or a diminished system lifetime.

In the extant literature, several techniques can be found to prepare ceramic particles used as a precursor for the subsequent molding and sintering of solid YSZ electrolytes [32]. However, the majority of these techniques, such as solution precursor plasma spraying, the sol–gel method, microwave synthesis, or sprayed solution drying, are either complicated or require sophisticated machinery [5,28,33–39]. In contrast, combustion synthesis or the thermal decomposition of suitable precursors represent rather simple and reliable methods for the preparation of YSZ powder with the desired dopant contents [22,24,40–42]. Among the most utilized processes, uniaxial powder compression and slurry casting are preferentially selected to form a solid electrolyte from powder precursors. Uniaxial compression is a fast and inexpensive molding method for the preparation of pellets of any shape. However, its drawback is its limited applicability, mainly for laboratory research purposes, because it produces relatively thick (>500 μm) pellets. On the other hand, the slurry casting method allows electrolytes to be produced around 100 μm thick, or even thinner [25–27,32,43]. However, this method is more complicated and expensive compared with uniaxial compression, due to the many process steps and the addition of dispersants. The last step of the conventional preparation of ceramic electrolytes involves particle sintering at a high temperature. From this information, it is clear that the method and conditions of YSZ powder preparation, as well as its subsequent sintering, will strongly impact the properties of the produced electrolyte, namely, its ionic conductivity and compactness or gas tightness.

Even though YSZ represents one of the most widespread electrolytes in SOC technology, comprehensive information on this aspect is lacking in the extant literature. It is thus the aim of this study to fill this gap.

The objective of this study is to present procedures for fabricating in-house YSZ electrolytes with suitable mechanical and morphological properties for utilization in SOCs. Different methods of YSZ powder preparation and shape molding techniques are compared. Combustion synthesis and the thermal decomposition of commercially available Zr/Y nitrates were chosen as fast and simple procedures to accomplish this task. The content of Y_2O_3 dopants varied in the range of 8 to 18 mol.%. This particular range of dopant content was chosen due to the following reasons:

- A number of researchers have investigated the properties of YSZ with very low dopant contents (i.e., 3 mol.%), confirming the very poor conductivity of such electrolytes [16,44–46]. On the other hand, a slight Y_2O_3 overdoping may be beneficial for solid oxide cell applications operating at lower temperatures [47–49]. Therefore, a lower limit of the range was chosen at a generally accepted optimum Y_2O_3 content to investigate potential property improvements with increasing the dopant content;
- On the other hand, excessive dopant content results in a decline in the YSZ conductivity. Y_2O_3 content of 18 mol.% was chosen as an upper dopant limit, because it clearly exceeds the optimum and falls into the declining conductivity range [47].

Commercially available powders and sintered electrolytes served to compare the electrolyte properties produced. Uniaxial compression or slurry casting were used to form the electrolyte pellet from the powders. These two techniques were chosen because they represent considerably different approaches. A direct comparison of the different powders and the two electrolyte formation techniques allows to set into relation the YSZ composition and preparation methods, an aspect that, until now, has been missing in the extant literature.

2. Experimental Section

The experimental workflow is displayed in Figure 1. The full description of individual steps is provided in the corresponding paragraphs.

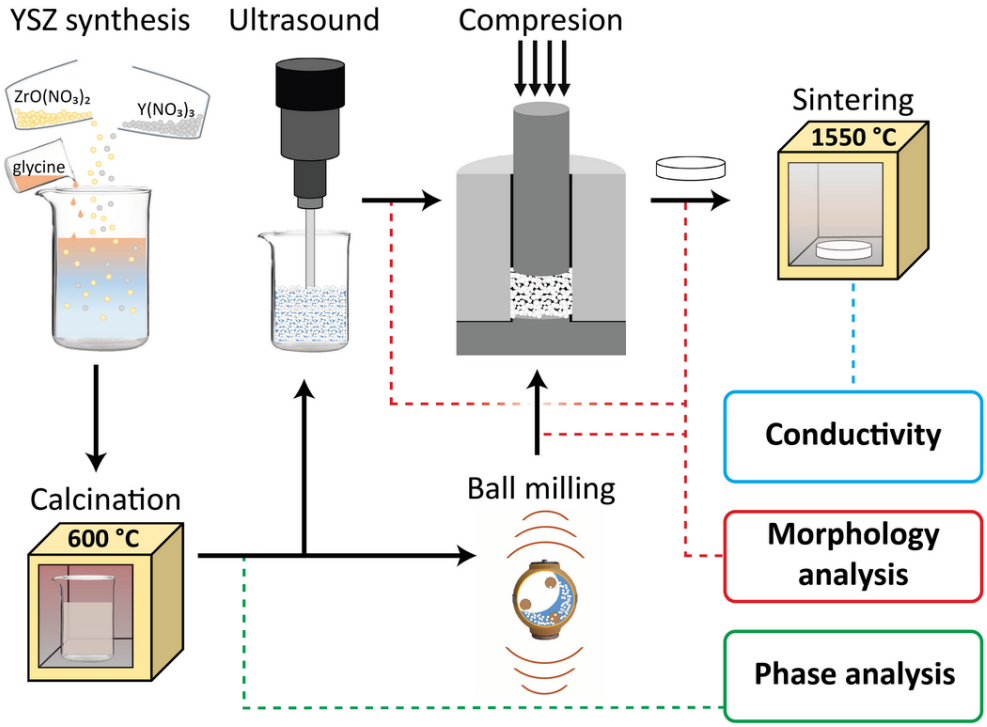

Figure 1. Graphical presentation of the experimental sequence.

2.1. Reference Materials

To compare multiple different fabrication approaches, a reference benchmark is necessary. Sintered polycrystalline YSZ pellets with a diameter of 25 mm and thickness of 0.15 mm and containing 8 mol.% of Y_2O_3 were purchased from KERAFOL GmbH. Additionally, polycrystalline YSZ powders (TZ-8YS, TZ-8YSB) containing 8 mol.% Y_2O_3 were purchased from Tosoh Corp. The only difference between these two powders is that the latter contains 3 wt.% of stearic acid as a binder agent for easier compression moldability.

2.2. YSZ Powder Synthesis

The following precursors were used for the in-house combustion synthesis of YSZ electrolyte powders: yttrium (III) nitrate hexahydrate (99.9%, ACROS Organics), Zirconium (IV) oxynitrate n-hydrate (99.5%, ACROS Organics) and glycine (A.G., PENTA).

The combustion synthesis procedure was described in our previous study [50]. In general, aqueous solutions of zirconium oxynitrate and yttrium nitrate were prepared, containing the desired ratios of both metal ions. Glycine, serving as a fuel for combustion, was added in the required amount. Then, the aqueous solution was boiled to remove excess water. The combustion synthesis was performed in a furnace at 400 °C for 12 h followed by calcination at 600 °C for 24 h.

In the case of thermal decomposition, the powders of ZrO^{2+} and Y^{3+} nitrates were mixed in the desired molar ratio. The prepared mixture was placed in a furnace. The decomposition took place at 600 °C for 24 h.

2.3. Solid Electrolyte Shape Molding from YSZ Powders

In-house-prepared powders were subjected to post-synthesis treatment. The first method was milling in a ball mill (Pulverisette 23, FRITSCH, Idar-Oberstein, Germany). A stainless-steel milling bowl cannot be utilized, because Cr is reported to be a possible catalytic poison for some electrode materials [51–53]. To avoid any contamination, a ZrO_2 milling bowl with ZrO_2 milling balls was used. The bowl was then filled with ethanol and the prepared YSZ powder. The milling was carried out at 50 revolutions per second for 15 min. The suspension of YSZ powder in ethanol was then dried at 80 °C for 24 h. The second post-synthesis treatment method was the application of ultrasound by means of an ultrasonic horn (Sonoplus VS 70 T horn, Sonoplus HD3100, BANDELIN, Berlin, Germany). A stainless-steel horn had to be utilized, regardless of the potential contamination of the YSZ powder. Nevertheless, due to the nature of the process, in this case, the risk of contamination may be considered to be insignificant. A fabricated powder was mixed with deionized water instead of ethanol to avoid possible ignition of the mixture due to the high-power output of the ultrasonic horn. The mixture (50 mL) was homogenized with a power output of 45 W for 15 min. After the ultrasound treatment, the aqueous suspension was dried at 80 °C for 24 h.

When uniaxial compression was used as a molding method, the corresponding YSZ powder was transferred into a circular mold and compressed at 68 MPa for 2 min (Trystom H-62 pressing machine) [54]. The amount of powder needed was calculated using the YSZ density to form pellets with an approximate thickness of 1 mm. Both in-house-synthesized as well as commercial TZ-8YSB powders were used for electrolyte pellet preparation by means of uniaxial compression.

In contrast to commercial slurry casting, where organic or even toxic dispersants are used, in the present case, the method was optimized to utilize water as a nontoxic, inexpensive dispersant. The aqueous suspension was prepared by mixing TZ-8YS and in-house powder after ultrasonic treatment with water in a 1:1.16 weight ratio, which has optimal properties for slurry casting. The suspension was then homogenized in a ball mill (Pulverisette 23, Fritsch) at 20 revolutions per second for 20 min. The prepared slurry was cast into a circular clay form located on a plaster support. A plaster support was chosen due to its hygroscopicity and smooth surface. These two properties are essential to quickly remove water content from ceramic suspension and to prepare as smooth and regular an

electrolyte surface as possible. In addition, the plaster support was chosen similarly to the whole method as an inexpensive material with a simple scale adjustment. The casted electrolyte was transferred directly into the furnace for sintering.

2.4. Sintering Procedure

The optimal sintering procedure depends on the YSZ powder preparation techniques and powder origin. Pellets prepared by the uniaxial compression of a commercial TZ-8YSB powder required sintering at 1360 °C for 6 h to achieve a sufficient degree of sintering, due to the homogeneity of the particle size distribution and easy sintering procedure declared by the manufacturer.

In contrast, pellets based on in-house-prepared powders required an elevated temperature to sinter, as discussed previously [50]. These electrolytes were sintered at 1360 °C for 6 h, and subsequently, the temperature was increased to 1550 °C for 12 h. The most complicated sintering protocol was applied to samples fabricated by slurry casting. At first, samples were heated to 1000 °C for 5 h. This temperature is not sufficient for the sufficient sintering degree of YSZ particles; however, it results in a slightly more rigid sample, still allowing potential shape processing when needed. To ensure the planarity of the sample during subsequent sintering, an alumina plate was placed over the samples. In the next step, the samples were sintered at 1360 °C for 6 h. Different sintering procedures resulted in two types of electrolytes. The first type was represented by electrolytes fabricated by the uniaxial compression of commercial and in-house-sintered powders resulting in approximately 0.8 mm thick pellets of 28 mm in diameter. The second type included electrolytes fabricated by slurry casting. They were less than 0.5 mm thick and had a diameter of 28 mm.

2.5. Determination of the Structure and Conductivity of the Samples

The structural and morphological characteristics of the materials were investigated after YSZ powder synthesis, as well as after electrolyte sintering. The YSZ powders were examined by means of X-ray diffraction (XRD; X'pert^3), X-ray fluorescence (XRF; ARL 9400), scanning electron microscopy (SEM, Hitachi S-4700, Hitachi, Tokyo, Japan), and laser scattering (Mastersizer 3000), utilizing the Mie scattering model to determine the composition, particle shape and size distribution. The inner volume structure of sintered electrolyte cross-sections was examined by means of scanning electron microscopy (SEM; Hitachi S4700).

For conductivity measurements, the in-house-prepared Ag_2O powder was mixed with ethylene glycol (A.G., PENTA) and homogenized in an ultrasonic bath for 30 min in order to prepare the suspension of the electrode ink. The electrode ink was then painted on both sides of sintered electrolytes and annealed at 800 °C for 4 h, resulting in the thermal decomposition of Ag_2O to Ag. The geometric area of the electrodes was calculated by image analysis using ImageJ software. The list of electrolytes whose conductivities were to be determined is summarized in Table 1.

Experimental apparatus was placed inside a furnace with an inbuilt thermocouple allowing precise temperature control. The experimental apparatus consisted of a quartz tube containing a fabricated cell, electrically contacted by a silver mesh. The exact operating temperature was verified by an additional type K thermocouple positioned close to the sample. Electrochemical impedance spectra (EIS) of the samples were recorded under an open-air atmosphere (1 bar) and in the temperature range of 400 to 800 °C using a programmable LCR-bridge (HAMEG HM8118). The EIS parameters were as follows: open circuit voltage; perturbing signal amplitude 50 mV; and frequency range of 200 kHz to 20 Hz. Spectra were recorded multiple times; the first measurement started at least 15 min after the desired temperature had stabilized. Results were evaluated by the method of equivalent circuits based on the work of Ahamer et al. [15]. To eliminate the impedance contribution of wires, blank spectra were recorded for a short-circuited apparatus with Ag

meshes for each temperature investigated. The Ohmic resistance contribution of the wiring was subtracted from the Ohmic resistance of each individual YSZ electrolyte sample.

Table 1. Various YSZ solid electrolytes used in this study for conductivity measurements.

Sample Name	Supplier	Y_2O_3 Content [mol.%]	Mono-/Poly-Crystalline	Synthesis Method	Preparation Method	Sintering Procedure
YSZ8—KERAFOL	KERAFOL	8	Poly	-	-	-
YSZ8—TZ-8YS (1360, casted)	TOSOH	8	Poly	-	slurry casting	1360 °C/6 h
YSZ8—TZ-8YSB (1360)	TOSOH	8	Poly	-	uniaxial compression	1360 °C/6 h
YSZ8—TZ-8YSB (1550)	TOSOH	8	Poly	-	uniaxial compression	1550 °C/24 h
YSZ8—m. (1550)	in-house	8	Poly	combustion + milled	uniaxial compression	1550 °C/24 h
YSZ13—(1360)	in-house	13	Poly	combustion	uniaxial compression	1360 °C/6 h
YSZ13—(1550)	in-house	13	Poly	combustion	uniaxial compression	1550 °C/24 h
YSZ13—m. (1550)	in-house	13	Poly	combustion + milled	uniaxial compression	1550 °C/24 h
YSZ13—US (1550)	in-house	13	Poly	combustion + ultrasonic horn	uniaxial compression	1550 °C/24 h
YSZ18—m. (1550)	in-house	18	Poly	combustion + milled	uniaxial compression	1550 °C/24 h

3. Results and Discussion

3.1. Determination of Structure and Composition of YSZ Powder

Initial results of YSZ powder preparation by means of combustion synthesis have been discussed previously [50]. In the present study, all synthesized powders were examined by means of XRD and XRF to confirm the desired crystalline structure and dopant content. XRD spectra shown in Figure 2 confirmed that commercial YSZ powder, as well as powders prepared by combustion or thermal decomposition synthesis, contained only a single phase. Diffraction line positions confirmed that all samples were of a cubic structure [10,21], thus proving homogeneity of the in-house-prepared powders. In addition, a pure crystalline structure was confirmed for all samples. XRF measurements confirmed the desired ZrO_2–Y_2O_3 composition according to the corresponding load. Thus, both methods are suitable for crystalline YSZ powder preparation of the desired dopant content.

3.2. Synthesis and Post-Synthesis Treatment of YSZ Powder

In our previous study, it was demonstrated that the sintering protocol suitable for commercially available powders (e.g., TZ-8YSB) is not sufficient for in-house-prepared powders, due to their large particles with an inhomogeneous geometry [50]. In the present study, an additional post-synthesis treatment was introduced to reduce the particle size and, in particular, to break down particle agglomerates formed during combustion synthesis. The combustion and thermal decomposition methods used in the present study prevented the formation of directly spherical particles similar to those of commercial powders. Nevertheless, the particle agglomerates created during synthesis (Figure 3a) could be disintegrated by a mechanical force or by applying sufficiently strong ultrasound.

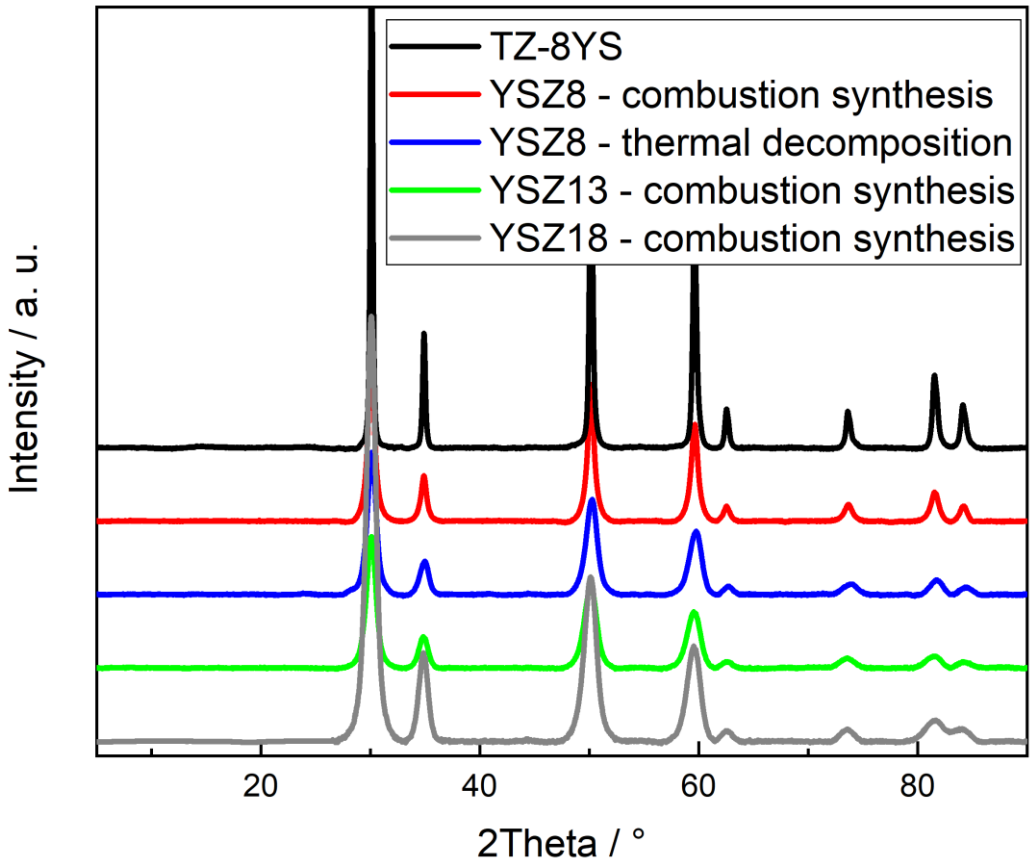

Figure 2. XRD analysis of YSZ commercial and in-house fabricated powders.

The impact of ball milling on the shape of YSZ particles is shown in Figure 3b. It is apparent that particle agglomerates had clearly disintegrated; however, the shape of particles remained unmodified, due to the hardness of the YSZ. Figure 3c shows YSZ powder particles after post-synthesis treatment by ultrasound. Similar to the ball milling result, the original particle agglomerates had disintegrated; moreover, the application of ultrasound resulted in even smaller YSZ particles than by ball milling. This result was confirmed by the particle size distribution obtained by means of laser scattering. Therefore, ultrasound is also a viable technique for YSZ powder treatment. Both methods resulted in electrolytes with equal properties, as discussed later. In this study, the ball milling method was preferentially used over the ultrasound treatment. This is because in the case of the ultrasonic treatment, commonly available ultrasonic baths cannot provide sufficient power output to disintegrate particles; thus, an ultrasound horn has to be used. It is not suitable for large volumes of synthesized powder processing, and the highly abrasive powder easily wears away the metallic horn. Additionally, ball milling offers a more flexible production capacity.

The thermal decomposition method represents the second approach chosen in this study. YSZ powder produced by this method consists of large crystallites rather than agglomerates, as shown in the SEM image in Figure 4a. In this case, the term crystallites instead of agglomerates is used, because the particles produced were difficult to disintegrate by post-synthesis treatment. This is demonstrated by an SEM image of a large particle which did not change its dimensions even after the ultrasonic post-synthesis powder treatment, as shown in Figure 4b. The ball milling treatment resulted in a nearly identical particle shape and size as in Figure 4b; thus, this image was omitted. This observation led to the conclusion that the thermal decomposition method is not suitable for production of YSZ powder targeted for further utilization in YSZ electrolyte membrane fabrication.

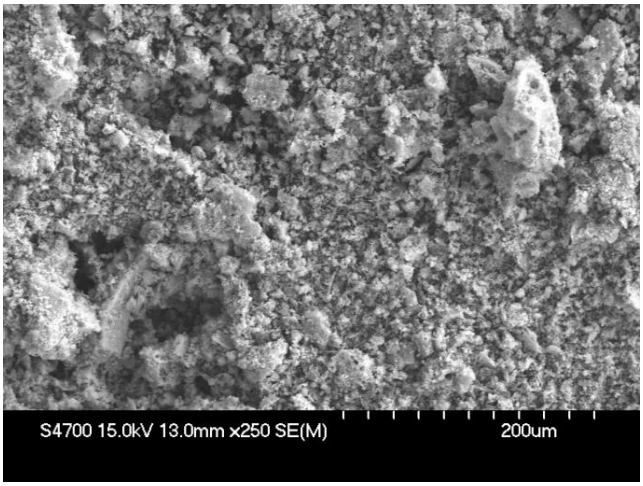

(**a**)

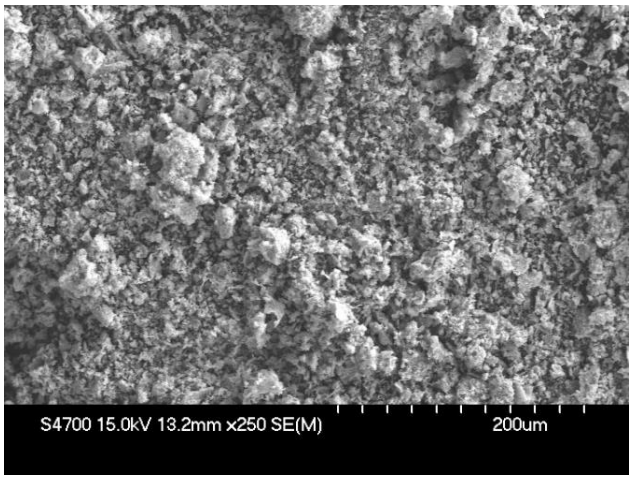

(**b**)

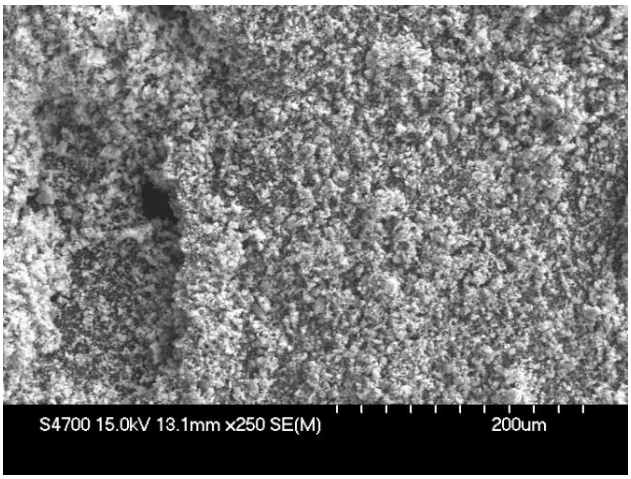

(**c**)

Figure 3. SEM images of YSZ particles containing 8 mol.% of Y_2O_3 prepared in-house by combustion method: (**a**) without post-synthesis treatment; treated by: (**b**) ball milling (50 rev./s; 15 min); (**c**) ultrasound horn (with a power output of 45 W for 15 min).

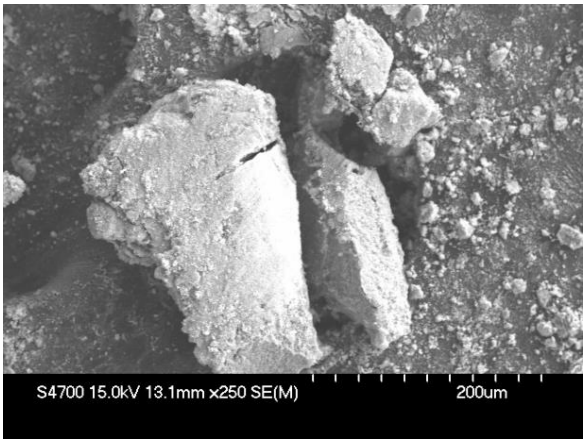

(**a**)

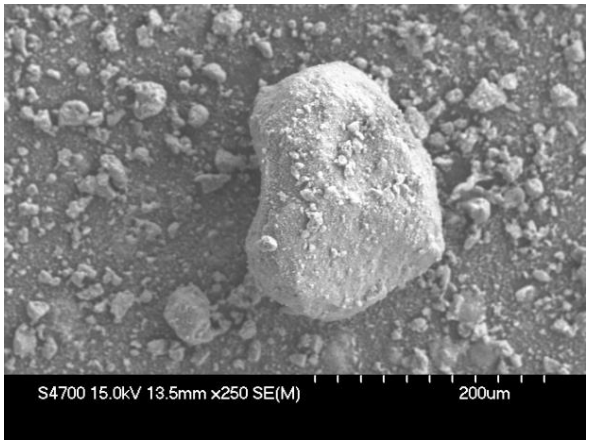

(**b**)

Figure 4. SEM images of YSZ particles containing 8 mol.% of Y_2O_3 prepared in-house by the thermal decomposition method: (**a**) without post-synthesis treatment; (**b**) treated by an ultrasound horn (with a power output of 45 W for 15 min).

In addition to the particle shape, the size distribution is a crucial parameter for a successful sintering process. Laser scattering was used to obtain this information. The results of particle size distribution for commercial powders (TZ-8YS and TZ-8YSB) are shown in Figure 5a. Consequently, for in-house-prepared powders based on the synthesis methods and post-synthesis treatments discussed, the results are shown in Figure 5b,c.

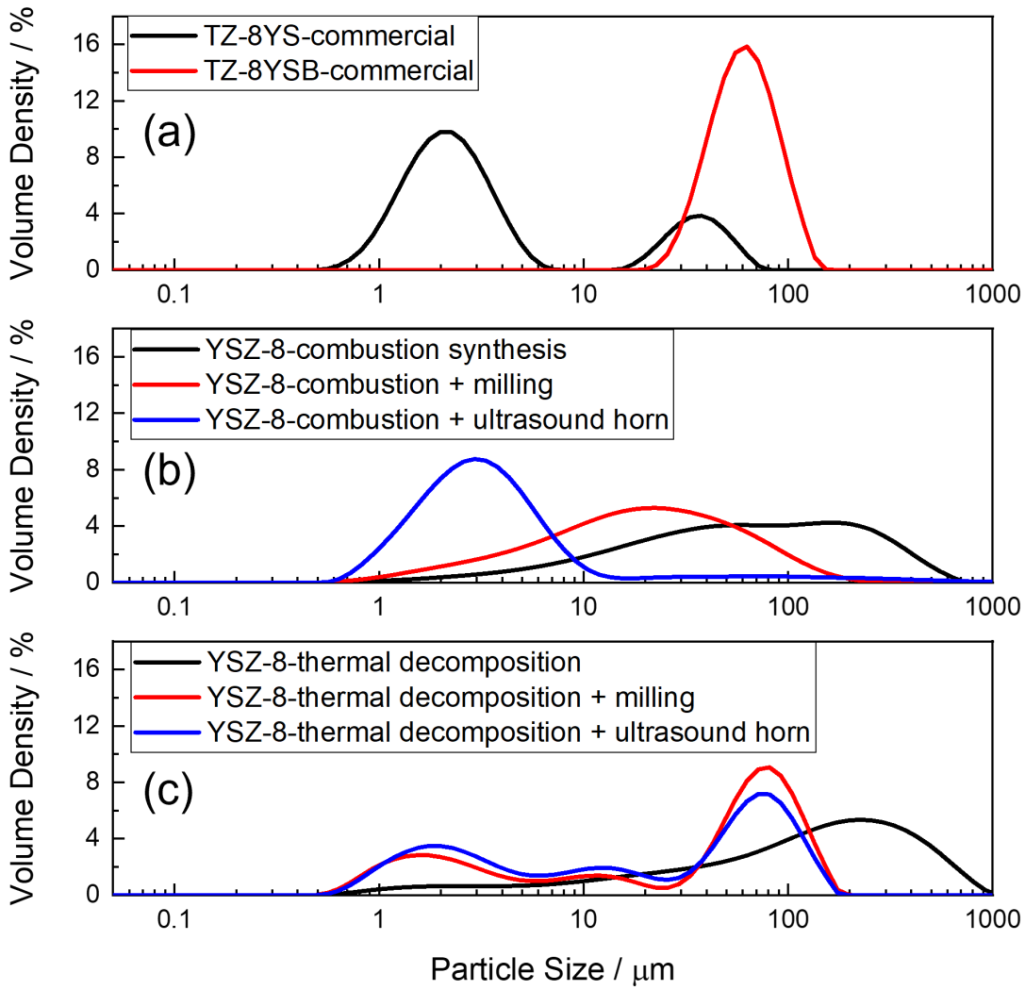

Figure 5. Particle size distribution of (**a**) commercially available powders TZ-8YS and TZ-8YSB; in-house-synthesized YSZ particles with 8 mol.% of Y_2O_3 prepared by: (**b**) combustion synthesis and subsequent post-synthesis treatment; (**c**) thermal decomposition and subsequent post-synthesis treatment.

Commercial powders exhibit a narrow particle size distribution. TZ-8YS powder shows bimodal size distribution, whereas TZ-8YSB is clearly unimodal. As already mentioned, the difference between the two powders consists solely of the presence of stearic acid (the binder) in the TZ-8YSB sample. The binder causes the smaller particles to be attached to the larger fraction, forming agglomerates. Due to the adherence strength, the larger particle fraction is unaffected by the presence of a binder. This arrangement results in the formal disappearance of the smaller fraction from the distribution diagram and a slight increase in the size of the larger fraction, as observed in Figure 5a.

In contrast to the commercial powders, as-prepared in-house-synthesized powders exhibited a significantly broader particle size distribution with a relatively large particle diameter. This is especially true in the case of powder prepared by the thermal decomposition of precursors (Figure 5c), as already shown in the SEM images. This preparation method results in crystallites with particles predominantly of 230 μm in diameter. Both post-synthesis treatment methods resulted in only slightly diminished particle sizes com-

pared with the untreated sample. Similarly to the combustion synthesis, small particles of approximately 3 μm in diameter were detached from larger particles. In the case of the thermal decomposition synthesis, however, the size of the main particle fraction remained largely unaffected by the post-synthesis treatment. In the case of powder prepared by combustion synthesis (Figure 5b), the YSZ particles had a broad size distribution with two dominant particle sizes. The smaller fraction was of approximately 40 μm, the larger one of approximately 200 μm in diameter. This is in agreement with the result obtained from the SEM images, reported above. The utilization of a ball mill results in a single fraction of particles (approximately 20 μm in diameter), although the size distribution is still relatively broad. The application of ultrasound horn produced the most uniform distribution of prepared powders, with the majority of particles being approximately 3 μm in diameter. In addition to uniform distribution, the size of these particles was comparable to the smaller particle fraction of TZ-8YS. Based on these observations, it is likely that combustion synthesis produced primarily agglomerated smaller particles rather than crystallites. Although alteration of the particle shape was not achieved, it was possible to efficiently disintegrate particle agglomerates by the chosen post-synthesis treatment.

3.3. Shape Molding and Sintering Process

In this study, two methods of electrolyte shape molding were considered: uniaxial compression and slurry casting. The first method discussed is uniaxial compression. It was shown that sintering at 1360 °C is clearly insufficient for in-house-prepared powders to form a compact and homogeneous electrolyte layer. A higher sintering temperature is necessary [50]. The best result was achieved for an electrolyte sintered at 1550 °C for 24 h. Nevertheless, traces of individual, poorly sintered particles remained visible at the cross-section of the electrolyte (Figure 6a). This degree of sintering was achieved for YSZ powder without post-synthesis treatment. The homogeneity of the sample was not sufficient to ensure mechanical stability and gas tightness sufficient for applications in SOCs [55]. Furthermore, the use of a powder with the broad size distribution of particles may result in an undesired, uneven thickness and irregular surface.

After post-synthesis treatment by milling or ultrasound of the YSZ powder prepared in-house, the sintered electrolyte exhibited an inner volume structure similar to that of the commercial powder electrolyte, as shown in Figure 6. In addition, the thickness of such an electrolyte is homogeneous due to the similar degree of contraction connected with the particles sintering over the electrolyte volume. Nevertheless, a higher frequency of pore occurrence is visible in the electrolyte cross-section, which is due to the non-uniform particle morphology before sintering. Examined samples, however, did not display open porosity or gas permeation through the electrolyte.

The slurry casting method is frequently used to fabricate thin electrolytes with a larger area. For the purpose of this study, commercial TZ-8YS powder characterized by the two distinct fractions of particle size was used to demonstrate the impact of the size distribution of broad YSZ powder particles on the properties of the resulting electrolyte. In contrast to uniaxial compression, in the case of slurry casting, the sedimentation of larger particles may occur during cast layer treatment. This results in an electrolyte layer with a gradient in the particle size, which is documented in Figure 7a. Homogenization to slurry just prior to the casting may partly help. This may limit the degree of sedimentation (especially for the relatively narrow particle size distribution), and thus increase the homogeneity of the sintered electrolyte (Figure 7b). Although the sedimentation effect was partly reduced, it could not be avoided completely. As a consequence of the particle size gradient in the layer, bending was observed during the sintering procedure due to the different volume contractions of the electrolyte parts consisting of different particle sizes. Thus, only powders with uniform particle size distribution clearly ensured the absence of any particle size gradient and formation of YSZ electrolyte with satisfactory properties. This was confirmed by the utilization of in-house-fabricated powder after ball milling treatment

(Figure 7c), where neither separation of particles according to their size, nor electrolyte bending was observed.

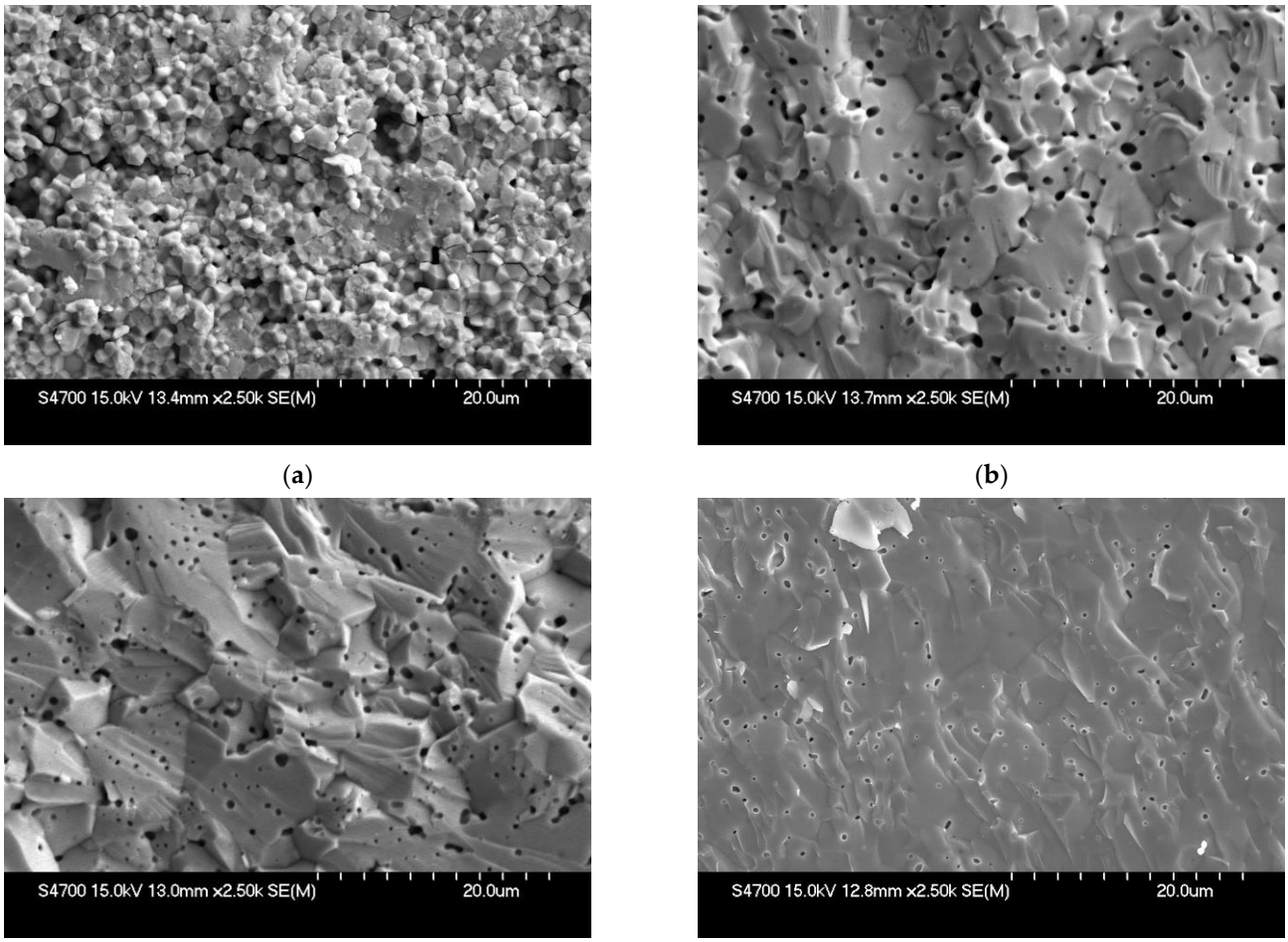

Figure 6. SEM images of the cross-section of sintered YSZ electrolytes, 8 mol.% of Y_2O_3, sintering temperature 1550 °C, sintering duration 24 h: (**a**) combustion synthesis—no post-synthesis treatment; (**b**) combustion synthesis—ball-milled; (**c**) combustion synthesis—ultrasound horn; (**d**) TZ-8YSB.

Although the optimized slurry casting allows production of thinner electrolytes when compared with those fabricated by the uniaxial compression, both methods resulted in electrolytes with equal conductivity, as discussed later. Thus, electrolytes fabricated by uniaxial compression are mainly utilized to avoid the limitations of particle sedimentation.

3.4. Conductivity Dependence of the YSZ Electrolyte on Temperature and Degree of Y_2O_3 Doping

Arrhenius plots were used to compare all the conductivity data recorded for the electrolytes under study. The dopant concentration and the electrolyte fabrication method are two main parameters discussed. Each electrolyte investigated (Table 1) was examined over a temperature range of 400 to 800 °C. At first, to compare the conductivity of the in-house-fabricated electrolyte with commercially available materials, electrolytes with 8 mol.% of Y_2O_3 dopant were investigated. All samples compared exhibited very similar conductivity regardless of the origin of the YSZ electrolyte (Figure 8). A slightly lower conductivity of the 'YSZ8—m. (1550)' sample can be explained by the marginal difference (<0.5%) in the dopant content in the synthesized YSZ powder. The expected linear dependence of $\ln(\sigma)$ vs. T^{-1} was observed for all samples tested. An inhomogeneous distribution of oxygen vacancies in YSZ lattices or the influence of intergrain conductivity would cause a

change in the activation energy (E_A) value, and consequently, the occurrence of different slopes in the Arrhenius plot [15,16,56]. It is thus possible to conclude that in-house-prepared YSZ powder, and also subsequently the electrolyte, have properties comparable with those of commercial products.

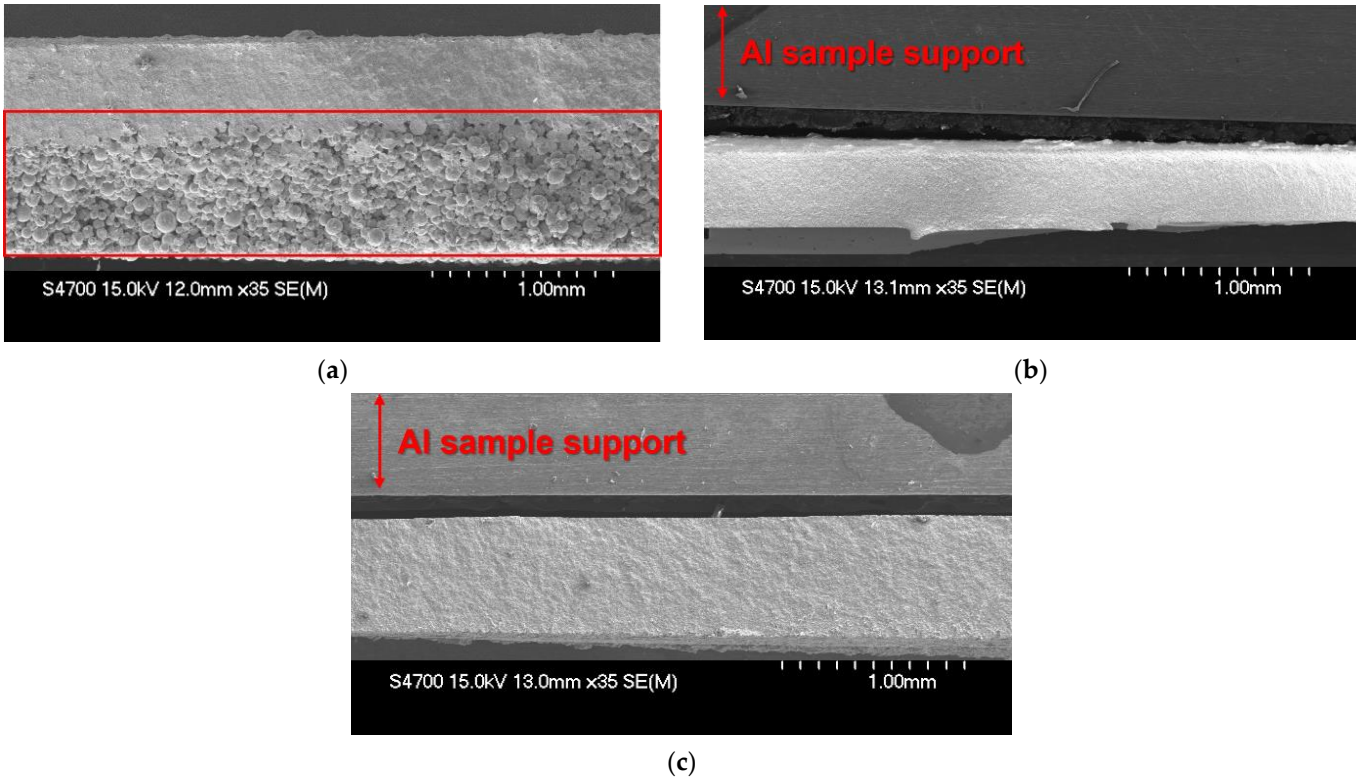

Figure 7. SEM images of the cross-section of sintered electrolytes, 8 mol.% Y_2O_3, fabricated by slurry casting: (**a**) TZ-8YS powder (1360 °C), the highlighted part of the electrolyte contains larger particles, which sedimented during the slurry casting; (**b**) TZ-8YS powder (1360 °C), freshly homogenized slurry; (**c**) in-house-fabricated powder (combustion synthesis—ball-milled; 1550 °C), a homogeneous electrolyte based on uniform particle size distribution.

In the next step, the impact of the synthesis method of YSZ powder and post-synthesis treatment was evaluated. The significant impact of different powder post-synthesis treatment and sintering protocols of YSZ powder is documented in Figure 9. Due to the more pronounced differences, samples containing 13 mol.% of Y_2O_3 were chosen to demonstrate the impact of the individual parameters. As per the discussed inner volume structure of the sintered electrolyte [50], the low sintering degree resulted in low conductivity of the electrolyte caused by the high resistance to the inter-grain contacts. The improved performance was achieved by elevating the sintering temperature (Figure 6a); however, the remaining inhomogeneity of the sintered electrolyte still limited the conductivity. The electrolyte based on milled powder and sintered at elevated temperature (Figure 6b) represented the result of the optimization of the in-house preparation of the electrolyte. This sample exhibited the highest conductivity of all the polycrystalline electrolytes, with 13 mol.% of Y_2O_3 under study. Identical results were achieved for electrolytes based on the ultrasonic post-synthesis treatment. This result documents the parity of both post-synthesis methods (Figure 6c), ensuring a homogeneous structure of the electrolyte with minimum void fraction and well-sintered YSZ particles.

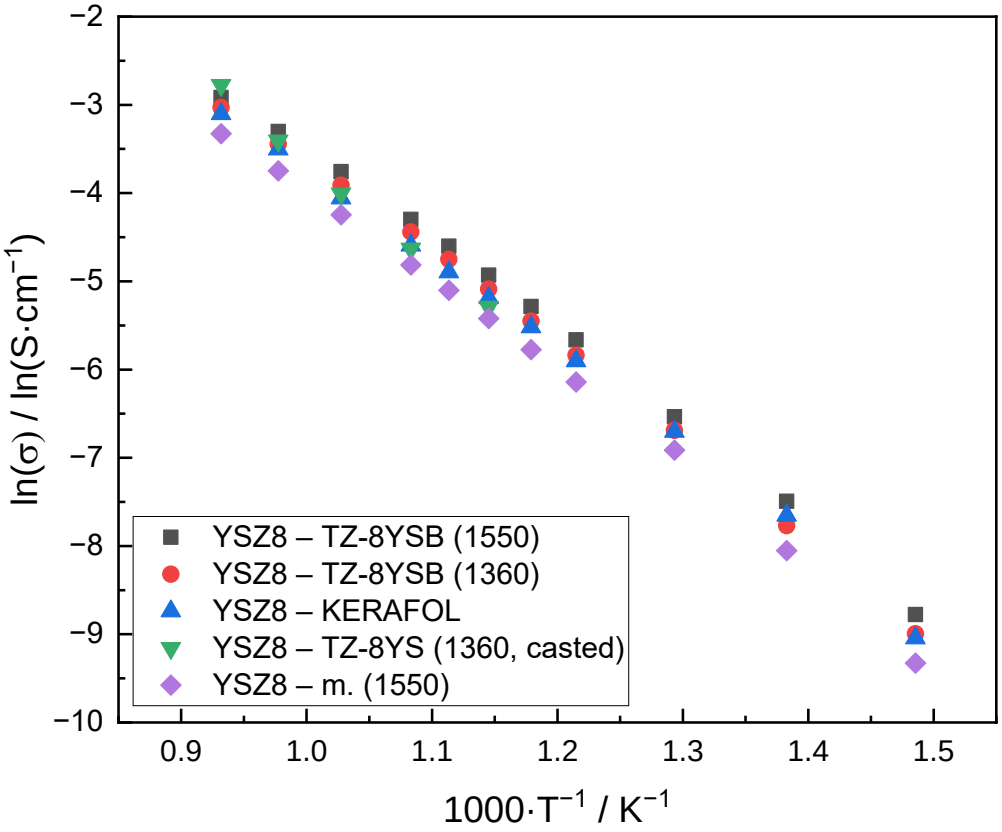

Figure 8. Arrhenius plot of the conductivity evaluated for polycrystalline YSZ samples containing 8 mol.% of Y_2O_3.

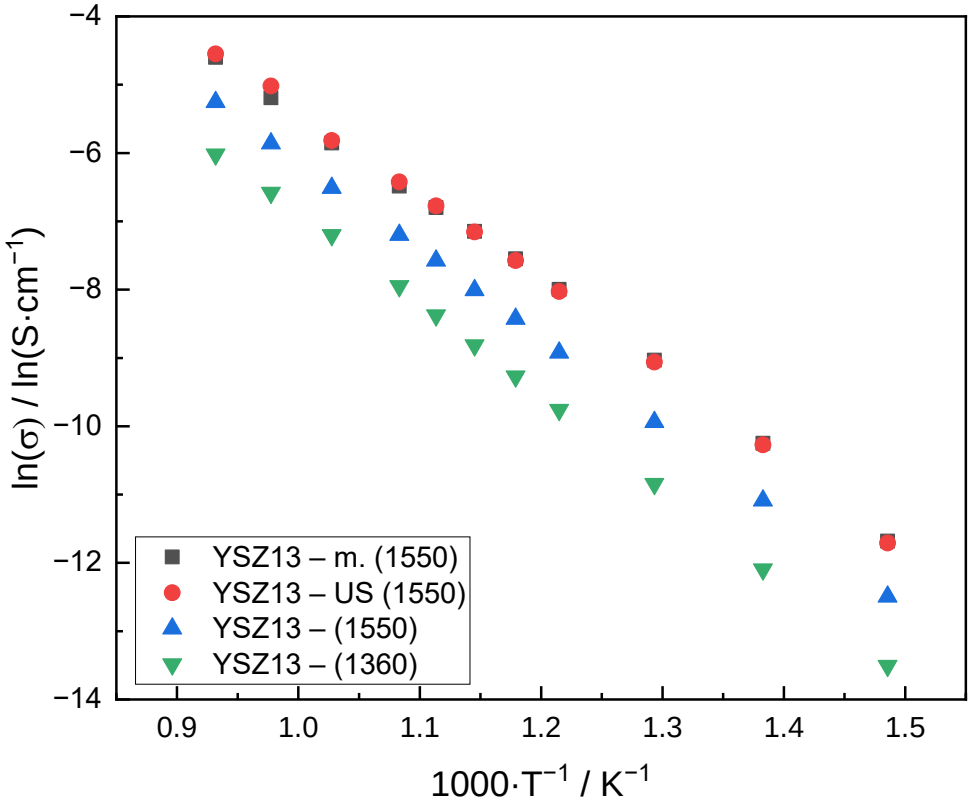

Figure 9. Arrhenius plot of the conductivity of in-house-fabricated polycrystalline YSZ samples with 13 mol.% of Y_2O_3.

The values of conductivity and activation energy for in-house electrolytes with different dopant content determined within the framework of this study are in agreement with those already reported [15,16,44]. Similar to data cited in the open literature, our samples exhibited the highest conductivity for YSZ electrolytes, with 8 mol.% of Y_2O_3 [20,44]. The conductivity of the samples diminished with increasing dopant contents, and the observed differences became less pronounced with increasing temperatures (shown in Figure 10). The conductivities determined for the evaluated samples with their respective activation energies (E_A) are summarized in Table 2.

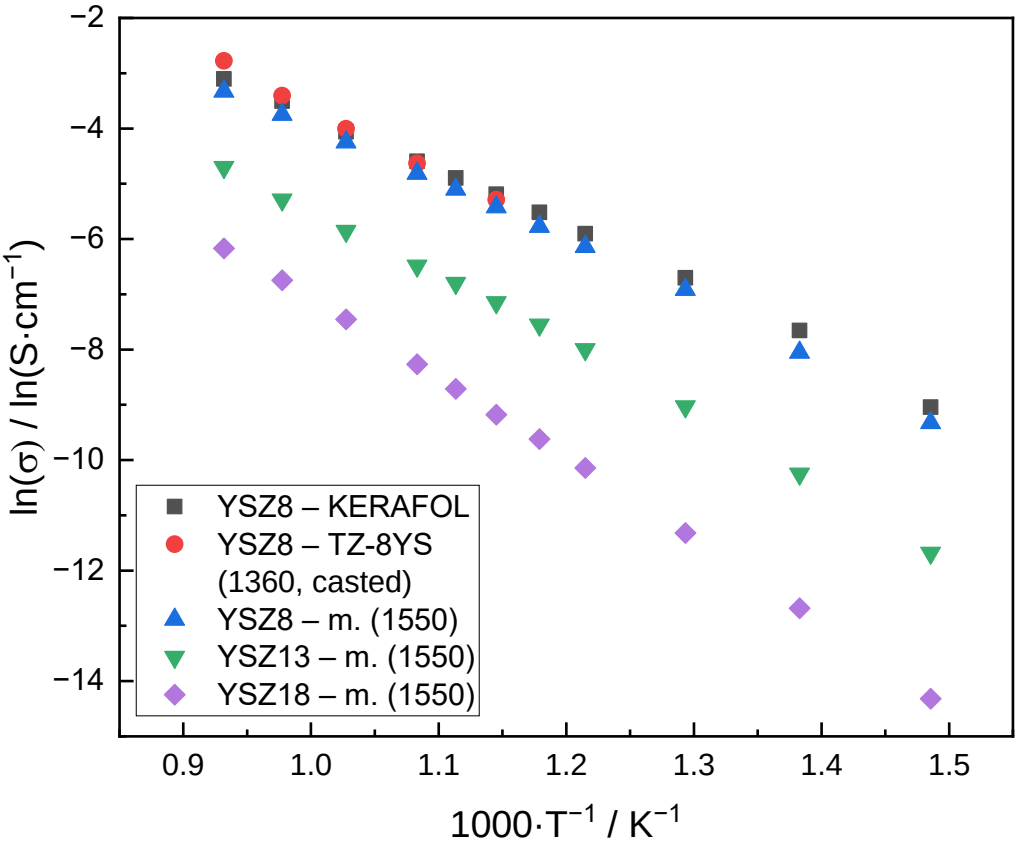

Figure 10. Arrhenius plot of the conductivity of all polycrystalline YSZ samples studied with varying Y_2O_3 dopant contents.

Table 2. YSZ electrolytes studied with their determined conductivity at 800 °C and activation energy (E_A).

Sample Name	σ 10^3/S·cm^{-1} @ 800 °C	E_A/kJ·mol^{-1}
'Y_2O_3 mol.%'—commercial name (sintering temperature)		
YSZ8—TZ-8YSB (1550)	54.12	87.9
YSZ8—TZ-8YSB (1360)	48.35	89.6
YSZ8—KERAFOL	44.91	87.4
YSZ8—TZ-8YS (1360, casted)	62.28	97.3
'Y_2O_3 mol.%'—post-synthesis method (sintering temperature)		
YSZ8—m. (1550)	35.88	89.1
YSZ13—m. (1550)	9.10	103.5
YSZ13—US (1550)	10.58	106.9
YSZ13—(1550)	5.22	108.2
YSZ13—(1360)	2.42	113.1
YSZ18—m. (1550)	2.10	122.3

4. Conclusions

This study compared simple methods of YSZ powder synthesis with varying Y_2O_3 contents suitable for the preparation of electrolytes in research laboratories. The main results can be summarized as follows:

- The combustion synthesis of precursors produced powders more suited for further processing than the thermal decomposition of the precursors;
- The combustion synthesis resulted in powder agglomerates that can be easily disintegrated during post-synthesis treatment to small particles of 3 μm in diameter and with a narrow size distribution;
- Small powder particles with uniform size distribution were essential in fabricating a dense YSZ electrolyte with minimal porosity, regardless of the molding technique used;
- The obtained conductivity values confirmed the assumed dependence of dopant content showing the maximum for the sample with 8 mol.% of Y_2O_3;
- All the studied samples displayed Arrhenius-like behavior in the whole range of temperatures.

Thus, this study clarifies the aspects to be considered during the in-house synthesis of YSZ electrolytes with a broad range of compositions. Above all, this study clarifies the impact of the individual fabrication steps on the properties of the resulting electrolyte. This is an important contribution to the community, because this detailed information was not available in the corresponding literature. It thus opens the way for studies focusing on the impact of YSZ electrolyte composition beyond the range offered by commercial suppliers.

Author Contributions: Conceptualization, M.C. and M.P.; methodology, M.C., N.A. and V.R.; validation, D.B., N.A. and V.R.; formal analysis, M.C.; investigation, N.A., V.R. and M.C.; resources, N.A. and V.R.; data curation, M.C.; writing—original draft preparation, M.C.; writing—review and editing, M.P. and K.B.; visualization, M.C.; supervision, M.P. and K.B.; project administration, K.B.; funding acquisition, K.B. All authors have read and agreed to the published version of the manuscript.

Funding: Czech Science Foundation (GACR): contract No: 19-14244J; University of Chemistry and Technology, Prague: grant No. A2_FCHT_2021_083; European Regional Development Fund Project "Fuel Cells with Low Platinum Content" (No. CZ.02.1.01/0.0/0.0/16_025/0007414).

Institutional Review Board Statement: Not applicable.

Informed Consent Statement: Not applicable.

Conflicts of Interest: The authors declare no conflict of interest.

References

1. Liu, Y.; Lao, L.E. Structural and electrical properties of ZnO-doped 8 mol% yttria-stabilized zirconia. *Solid State Ion.* **2006**, *177*, 159–163. [CrossRef]
2. Fergus, J.W. Electrolytes for solid oxide fuel cells. *J. Power Sources* **2006**, *162*, 30–40. [CrossRef]
3. Brodnikovska, I.; Korsunska, N.; Khomenkova, L.; Polishchuk, Y.; Lavoryk, S.; Brychevskyi, M.; Brodnikovskyi, Y.; Vasylyev, O. Grains, grain boundaries and total ionic conductivity of 10Sc1CeSZ and 8YSZ solid electrolytes affected by crystalline structure and dopant content. *Mater. Today-Proc.* **2019**, *6*, 79–85. [CrossRef]
4. Ren, C.; He, Y.D.; Wang, D.R. Fabrication and Characteristics of YSZ–YSZ/Al_2O_3 Double-Layer TBC. *Oxid. Met.* **2011**, *75*, 325–335. [CrossRef]
5. Jena, P.; Patro, P.K.; Sinha, A.; Lenka, R.K.; Singh, A.K.; Mahata, T.; Sinha, P.K. Hydrothermal Synthesis and Characterization of an Apatite-Type Lanthanum Silicate Ceramic for Solid Oxide Fuel Cell Electrolyte Applications. *Energy Technol.* **2018**, *6*, 1739–1746. [CrossRef]
6. Tao, Z.; Fu, M.; Liu, Y.; Gao, Y.; Tong, H.; Hu, W.; Lei, L.; Bi, L. High-performing proton-conducting solid oxide fuel cells with triple-conducting cathode of $Pr_{0.5}Ba_{0.5}(Co_{0.7}Fe_{0.3})O_{3-\delta}$ tailored with W. *Int. J. Hydrogen Energy* **2022**, *47*, 1947–1953. [CrossRef]
7. Tao, Z.; Fu, M.; Liu, Y. A mini-review of carbon-resistant anode materials for solid oxide fuel cells. *Sustain. Energy Fuels* **2021**, *5*, 5420–5430. [CrossRef]
8. Ma, S.; Lin, M.; Lin, T.E.; Lan, T.; Liao, X.; Maréchal, F.; Van Herle, J.; Yang, Y.; Dong, C.; Wang, L. Fuel cell-battery hybrid systems for mobility and off-grid applications: A review. *Renew. Sustain. Energy Rev.* **2021**, *135*, 110119. [CrossRef]

9. Ye, L.; Xie, K. High-temperature electrocatalysis and key materials in solid oxide electrolysis cells. *J. Energy Chem.* **2021**, *54*, 736–745. [CrossRef]
10. Khan, M.Z.; Song, R.H.; Mehran, M.T.; Lee, S.B.; Lim, T.H. Controlling cation migration and inter-diffusion across cathode/interlayer/electrolyte interfaces of solid oxide fuel cells: A review. *Ceram. Int.* **2021**, *47*, 5839–5869. [CrossRef]
11. Sengupta, P.; Bhattacharjee, A.; Maiti, H.S. Zirconia: A Unique Multifunctional Ceramic Material. *Trans. Indian Inst. Met.* **2019**, *72*, 1981–1998. [CrossRef]
12. Carda, M.; Budáč, D.; Paidar, M.; Bouzek, K. Current trends in the description of lanthanum strontium manganite oxygen electrode reaction mechanism in a high-temperature solid oxide cell. *Curr. Opin. Electrochem.* **2022**, *31*, 100852. [CrossRef]
13. Petot-Ervas, G.; Rizea, A.; Petot, C. Electrode materials, interface processes and transport properties of yttria-doped zirconia. *Ionics* **1997**, *3*, 405–411. [CrossRef]
14. Wu, S.; Xu, X.; Li, X.; Bi, L. High-performance proton-conducting solid oxide fuel cells using the first-generation Sr-doped LaMnO3 cathode tailored with Zn ions. *Sci. China Mater.* **2022**, *65*, 675–682. [CrossRef]
15. Ahamer, C.; Opitz, A.K.; Rupp, G.M.; Fleig, J. Revisiting the temperature dependent ionic conductivity of yttria stabilized zirconia (YSZ). *J. Electrochem. Soc.* **2017**, *164*, F790–F803. [CrossRef]
16. Badwal, S.P.S. Zirconia-based solid electrolytes: Microstructure, stability and ionic conductivity. *Solid State Ion.* **1992**, *52*, 23–32. [CrossRef]
17. Kharton, V.; Marques, F.; Atkinson, A. Transport properties of solid oxide electrolyte ceramics: A brief review. *Solid State Ion.* **2004**, *174*, 135–149. [CrossRef]
18. Strickler, D.W.; Carlson, W.G. Ionic Conductivity of Cubic Solid Solutions in the System CaO—Y_2O_3—ZrO_2. *J. Am. Ceram. Soc.* **1964**, *47*, 122–127. [CrossRef]
19. Xue, Q.N.; Huang, X.W.; Wang, L.G.; Zhang, H.; Zhang, J.X. Computational and Experimental Investigations of Defect Interaction and Ionic Conductivity in Doped Zirconia. *Phys. Rev. Appl.* **2018**, *10*, 9. [CrossRef]
20. Tsipis, E.V.; Kharton, V.V. Electrode materials and reaction mechanisms in solid oxide fuel cells: A brief review: I Performance-determining factors. *J. Solid State Electrochem.* **2008**, *12*, 1039–1060. [CrossRef]
21. Tan, Z.H.; Guo, X. Synthesis and characterization of highly dispersed YSZ particles with diameter $\leq$ 5 nm. *Ceram. Int.* **2015**, *41*, 4953–4958. [CrossRef]
22. Kaus, I.; Dahl, P.I.; Mastin, J.; Grande, T.; Einarsrud, M.A. Synthesis and characterization of nanocrystalline YSZ powder by smoldering combustion synthesis. *J. Nanomater.* **2006**, *2006*, 049283. [CrossRef]
23. Syed, A.A.; Ilhan, Z.; Arnold, J.; Schiller, G.; Weckmann, H. Improving plasma-sprayed yttria-stabilized zirconia coatings for solid oxide fuel cell electrolytes. *J. Therm. Spray Technol.* **2006**, *15*, 617–622. [CrossRef]
24. Reddy, B.S.B.; Mal, I.; Tewari, S.; Das, K.; Das, S. Aqueous combustion synthesis and characterization of nanosized tetragonal zirconia single crystals. *Metall. Mater. Trans. A* **2007**, *38*, 1786–1793. [CrossRef]
25. Bitterlich, B.; Lutz, C.; Roosen, A. Rheological characterization of water-based slurries for the tape casting process. *Ceram. Int.* **2002**, *28*, 675–683. [CrossRef]
26. Boaro, M.; Vohs, J.M.; Gorte, R.J. Synthesis of highly porous yttria-stabilized zirconia by tape-casting methods. *J. Am. Ceram. Soc.* **2003**, *86*, 395–400. [CrossRef]
27. Xin, X.; Lü, Z.; Zhu, Q.; Huang, X.; Su, W. Fabrication of dense YSZ electrolyte membranes by a modified dry-pressing using nanocrystalline powders. *J. Mater. Chem.* **2007**, *17*, 1627–1630. [CrossRef]
28. Hu, L.; Wang, C.A.; Huang, Y.; Sun, C.; Lu, S.; Hu, Z. Control of pore channel size during freeze casting of porous YSZ ceramics with unidirectionally aligned channels using different freezing temperatures. *J. Eur. Ceram. Soc.* **2010**, *30*, 3389–3396. [CrossRef]
29. Van Herle, J.; McEvoy, A.J.; Thampi, K.R. Conductivity measurements of various yttria-stabilized zirconia samples. *J. Mater. Sci.* **1994**, *29*, 3691–3701. [CrossRef]
30. Sasongko, M.N.; Perdana, F.; Wijayanti, W. Analysis of the Effect of Ionic Conductivity of Electrolyte Materials on the Solid Oxide Fuel Cell Performance. *East.-Eur. J. Enterp. Technol.* **2021**, *3*, 41–52. [CrossRef]
31. Jiang, J.; Hertz, J.L. On the variability of reported ionic conductivity in nanoscale YSZ thin films. *J. Electroceram.* **2014**, *32*, 37–46. [CrossRef]
32. Li, K. Preparation of Ceramic Membranes. In *Ceramic Membranes for Separation and Reaction*; John Wiley & Sons, Ltd.: Hoboken, NJ, USA, 2007; pp. 21–57. [CrossRef]
33. Enríquez-Martínez, A.; Mosqueda-Laffita, Y.; Aguilar-Frutis, M.; Alarcón-Flores, G.; Grima-Gallardo, P.; León-Ramírez, H.; Pérez-Cappe, E. YSZ nanoparticles and thin films prepared in a single crystallization step at low temperature. *Mater. Res. Express* **2019**, *6*, 126412. [CrossRef]
34. Han, M.; Tang, X.; Yin, H.; Peng, S. Fabrication, microstructure and properties of a YSZ electrolyte for SOFCs. *J. Power Sources* **2007**, *165*, 757–763. [CrossRef]
35. Cho, G.Y.; Noh, S.; Lee, Y.H.; Ji, S.; Hong, S.W.; Koo, B.; An, J.; Kim, Y.B.; Cha, S.W. Properties of nanostructured undoped ZrO_2 thin film electrolytes by plasma enhanced atomic layer deposition for thin film solid oxide fuel cells. *J. Vac. Sci. Technol. A Vac. Surf. Film.* **2016**, *34*, 01A151. [CrossRef]
36. Kim, S.-G.; Yoon, S.P.; Nam, S.W.; Hyun, S.-H.; Hong, S.-A. Fabrication and characterization of a YSZ/YDC composite electrolyte by a sol–gel coating method. *J. Power Sources* **2002**, *110*, 222–228. [CrossRef]

37. Menzler, N.H.; Tietz, F.; Uhlenbruck, S.; Buchkremer, H.P.; Stöver, D. Materials and manufacturing technologies for solid oxide fuel cells. *J. Mater. Sci.* **2010**, *45*, 3109–3135. [CrossRef]
38. Izumi, M.; Sasahara, N. Effect of pre-sintering of raw material powder on properties of solid oxide fuel cell electrolyte prepared by dip-coating method. *J. Ceram. Soc. Jpn.* **2010**, *118*, 944–947. [CrossRef]
39. Park, J.; Paek, J.Y.; Chang, I.; Ji, S.; Cha, S.W.; Oh, S.I. Pulsed laser deposition of Y-doped BaZrO3 thin film as electrolyte for low temperature solid oxide fuel cells. *CIRP Ann.-Manuf. Technol.* **2013**, *62*, 563–566. [CrossRef]
40. Sherikar, B.N.; Sahoo, B.; Umarji, A.M. Effect of fuel and fuel to oxidizer ratio in solution combustion synthesis of nanoceramic powders: MgO, CaO and ZnO. *Solid State Sci.* **2020**, *109*, 106426. [CrossRef]
41. Singh, K.L.; Singh, G.; Sharma, P.; Mago, S.; Singh, A.P. Effect of fuel/nitrate molar ratio on the properties of nio-YSZ nanocomposites as anode material for solid oxide fuel cell synthesised by combustion method. *Int. J. Nanopart.* **2018**, *10*, 298–311. [CrossRef]
42. Hao, S.J.; Wang, C.; Liu, T.L.; Mao, Z.M.; Mao, Z.Q.; Wang, J.L. Fabrication of nanoscale yttria stabilized zirconia for solid oxide fuel cell. *Int. J. Hydrogen Energy* **2017**, *42*, 29949–29959. [CrossRef]
43. Sanson, A.; Pinasco, P.; Roncari, E. Influence of pore formers on slurry composition and microstructure of tape cast supporting anodes for SOFCs. *J. Eur. Ceram. Soc.* **2008**, *28*, 1221–1226. [CrossRef]
44. Filal, M.; Petot, C.; Mokchah, M.; Chateau, C.; Carpentier, J.L. Ionic conductivity of yttrium-doped zirconia and the "composite effect". *Solid State Ion.* **1995**, *80*, 27–35. [CrossRef]
45. Uchida, H.; Yoshida, M.; Watanabe, M. Effects of ionic conductivities of zirconia electrolytes on polarization properties of platinum anodes in solid oxide fuel cells. *J. Phys. Chem.* **1995**, *99*, 3282–3287. [CrossRef]
46. Badwal, S.P.S.; Ciacchi, F.T. Oxygen-ion conducting electrolyte materials for solid oxide fuel cells. *Ionics* **2000**, *6*, 1–21. [CrossRef]
47. Cho, G.Y.; Lee, Y.H.; Yu, W.; An, J.; Cha, S.W. Optimization of Y_2O_3 dopant concentration of yttria stabilized zirconia thin film electrolyte prepared by plasma enhanced atomic layer deposition for high performance thin film solid oxide fuel cells. *Energy* **2019**, *173*, 436–442. [CrossRef]
48. Sik Son, K.; Bae, K.; Woo Kim, J.; Suk Ha, J.; Hyung Shim, J. Ion conduction in nanoscale yttria-stabilized zirconia fabricated by atomic layer deposition with various doping rates. *J. Vac. Sci. Technol. A Vac. Surf. Film.* **2013**, *31*, 01A107. [CrossRef]
49. Chao, C.C.; Kim, Y.B.; Prinz, F.B. Surface modification of yttria-stabilized zirconia electrolyte by atomic layer deposition. *Nano Lett.* **2009**, *9*, 3626–3628. [CrossRef]
50. Carda, M.; Adamová, N.; Budáč, D.; Paidar, M.; Bouzek, K. Preparation Protocol and Properties of YSZ Ceramic Electrolytes for Solid Oxide Cells. *ECS Trans.* **2021**, *105*, 97–105. [CrossRef]
51. Konysheva, E.Y. The Effect of Chromium Oxide on the Conductivity of $Ce_{0.9}Gd_{0.1}O_2$, a Solid-Oxide Fuel Cell Electrolyte. *Russ. J. Electrochem.* **2018**, *54*, 471–480. [CrossRef]
52. Tu, H.; Stimming, U. Advances, aging mechanisms and lifetime in solid-oxide fuel cells. *Eight Ulm. Electrochem. Tage* **2004**, *127*, 284–293. [CrossRef]
53. Schuler, J.A.; Yokokawa, H.; Calderone, C.F.; Jeangros, Q.; Wuillemin, Z.; Hessler-Wyser, A.; Van Herle, J. Combined Cr and S poisoning in solid oxide fuel cell cathodes. *J. Power Sources* **2012**, *201*, 112–120. [CrossRef]
54. Lieberzeit, J. Preparation of Electrolyte for High Temperature Water Electrolysis. Bachelor's Thesis, University of Chemistry and Technology Prague, Prague, Czech Republic, 2015.
55. Atkinson, A. Solid Oxide Fuel Cell Electrolytes-Factors Influencing Lifetime. In *Solid Oxide Fuel Cell Lifetime and Reliability: Critical Challenges in Fuel Cells*; Elsevier Inc.: Amsterdam, The Netherlands, 2017; pp. 19–35. [CrossRef]
56. Vendrell, X.; West, A.R. Electrical properties of yttria-stabilized zirconia, YSZ single crystal: Local AC and long range DC conduction. *J. Electrochem. Soc.* **2018**, *165*, F966–F975. [CrossRef]